1996ApJ...466..158S

THE ASTROPHYSICAL JOURNAL, 466:158–168, 1996 July 20
© 1996. The American Astronomical Society. All rights reserved. Printed in U.S.A.

THE EVOLUTION OF THE CENTIMETER–SUBMILLIMETER SPECTRUM OF 3C 345 DURING OUTBURST

J. A. STEVENS[1] AND S. J. LITCHFIELD[2]
Centre for Astrophysics, University of Central Lancashire, Preston PR1 2HE, England, UK
E. I. ROBSON[3]
Joint Astronomy Centre, 660 North A'ohōkū Place, University Park, Hilo, HI 96720
T. V. CAWTHORNE
Centre for Astrophysics, University of Central Lancashire, Preston PR1 2HE, England, UK
M. F. ALLER, H. D. ALLER, AND P. A. HUGHES
Astronomy Department, University of Michigan, Ann Arbor, MI 48109-1090
AND
M. C. H. WRIGHT
Radioastronomy Laboratory, University of California, Berkeley, CA 94720
Received 1995 October 2; accepted 1996 February 2

ABSTRACT

Monitoring data between 375 and 4.8 GHz are presented for the blazar 3C 345 between 1989 and 1995, during which period the source flared. The multifrequency light curves are used to construct snapshot spectra that span the synchrotron self-absorption turnover frequency. After subtraction of the underlying quiescent level, the flare spectrum is isolated and followed during the outburst. The evolution of the turnover frequency (ν_m) with turnover flux (S_m) is examined and compared with the predictions of the Marscher & Gear shocked-jet model. We find that the flare spectrum is well fitted by a homogeneous synchrotron curve for at least 2 yr after the initial rise in flux. The high-frequency optically thin section of this spectrum is observed to steepen with time. The extent of this steepening suggests that little reacceleration is occurring in the shock. We find that a power law is a remarkably good approximation to the observed trend of S_m with ν_m. The turn over moves smoothly toward lower frequency with time, as expected from an emitting region that is expanding. Furthermore, this movement is observed to slow down with time, as predicted by the model. Initially, the turnover flux rises and then decays with a power-law index of ~ 1.0. This decay is interrupted by a second rise, which also decays with an index of ~ 1.0. It is found that the initial rise corresponds to the expansion phase, with the jet bending toward the line of sight rather than to the Compton or synchrotron phases of the model. Furthermore, the decays can only be reconciled with the model if the jet is assumed to be nonadiabatic or if it curves away from the line of sight during this period. The implied magnetic field orientation is parallel to the shock front, as expected from compression of the underlying field. This finding is supported by the total polarization data that suggest that the outbursts depolarize the total emission, which, during quiescent periods, is significantly polarized in a direction approximately perpendicular ($B_{\|}$) to the jet axis.

Subject headings: galaxies: jets — polarization — quasars: individual (3C 345) — radiation mechanisms: nonthermal — radio continuum: galaxies

1. INTRODUCTION

3C 345 is a typical blazar, exhibiting variability in all wave bands (e.g., Aller et al. 1985; Webb et al. 1988; Unwin et al. 1994), high levels of optical and radio polarization (e.g., Angel & Stockman 1980; Brown, Roberts, & Wardle 1994), and superluminal VLBI component speeds (e.g., Moffet et al. 1972). The radio jet exhibits significant bending on all scales that have been probed with VLBI, the effect being more pronounced close to the core (e.g., Bååth et al. 1992). The study of blazars is central to understanding the mechanisms responsible for variability in radio-loud active galactic nuclei. There is ample evidence to show that the optical–radio continuum emission from blazars is produced by the synchrotron mechanism. Furthermore, shock waves propagating along a relativistic jet, aligned toward the line of sight of the observer, produce the observed flux variability and VLBI component expansions. Models incorporating these ideas have proved successful in interpreting the infrared–radio outbursts of blazars (e.g., Marscher & Gear 1985; Hughes, Aller, & Aller 1985, 1989a, b; Cawthorne & Wardle 1988). Further observations are required, however, to test and improve the models, especially the Marscher & Gear model, which makes predictions for the early stages of flare evolution.

After a period of low-level emission during 1989 and 1990, 3C 345 flared dramatically during 1991, reaching a maximum at millimeter wavelengths toward the end of the year and then declining through 1993 and 1994. Multifrequency data (radio X-ray) for this flare have been presented by Webb et al. (1994). In this paper, submillimeter, millimeter, and centimeter monitoring data over the period 1989–1995 are used to study the variability of 3C 345 during this outburst. Observations at these wavelengths

[1] Present address: Joint Astronomy Centre, 660 North A'ohōkū Place, University Park, Hilo, HI 96720.
[2] Present address: University of Crete, Physics Department, 714 09 Heraklion, Crete, Greece.
[3] Also at the Centre for Astrophysics, University of Central Lancashire, Preston PR1 2HE, England, UK.

© American Astronomical Society • Provided by the NASA Astrophysics Data System

1996ApJ...466..158S

span the turnover region of the synchrotron spectrum, where the radiation becomes self-absorbed and are ideal for testing the predictions of the Marscher & Gear model.

2. OBSERVATIONS

Millimeter and submillimeter monitoring data have been collected at the 15 m James Clerk Maxwell Telescope (JCMT) since 1989. These observations at frequencies of 375, 270, 230, and 150 GHz (0.8, 1.1, 1.3, and 2.0 mm, respectively) were taken with the ^{3}He-cooled facility bolometer UKT14 (Duncan et al. 1990). Standard observing techniques were used (see, e.g., Robson et al. 1993), and the observations were calibrated against either the planets or the JCMT secondary calibrators (Sandell 1994). The data reduction techniques are described by Stevens & Robson (1994) and Sandell (1994). Data taken prior to 1994 have been published elsewhere (Stevens et al. 1994). Data at 90 GHz (3.3 mm) were taken from the literature (Steppe et al. 1993) and were also obtained from the Berkeley-Illinois-Maryland Array (BIMA) at Hat Creek, California, where 3C 345 is used as a gain calibrator. The flux density at 90 GHz is calibrated from observations of the planets using surface brightness values given by Ulich (1981). The 37 and 22 GHz monitoring data are from Metsähovi Radio Research Station (MRRS), Finland, where a large sample of active galaxies are observed on a regular basis (see Teräsranta et al. 1992). These data have also been published previously (Stevens et al. 1994). Data at 14.5, 8.0, and 4.8 GHz were taken with the 26 m radio antenna of the University of Michigan, again as part of a larger monitoring program (see Aller et al. 1985).

3. RESULTS

3.1. *The Light Curves*

The 3C 345 light curves are presented in Figure 1. A large outburst that persists for about 4 yr dominates the light curves at all of the monitoring frequencies. There is evidence for this outburst to be complex in structure, and it is

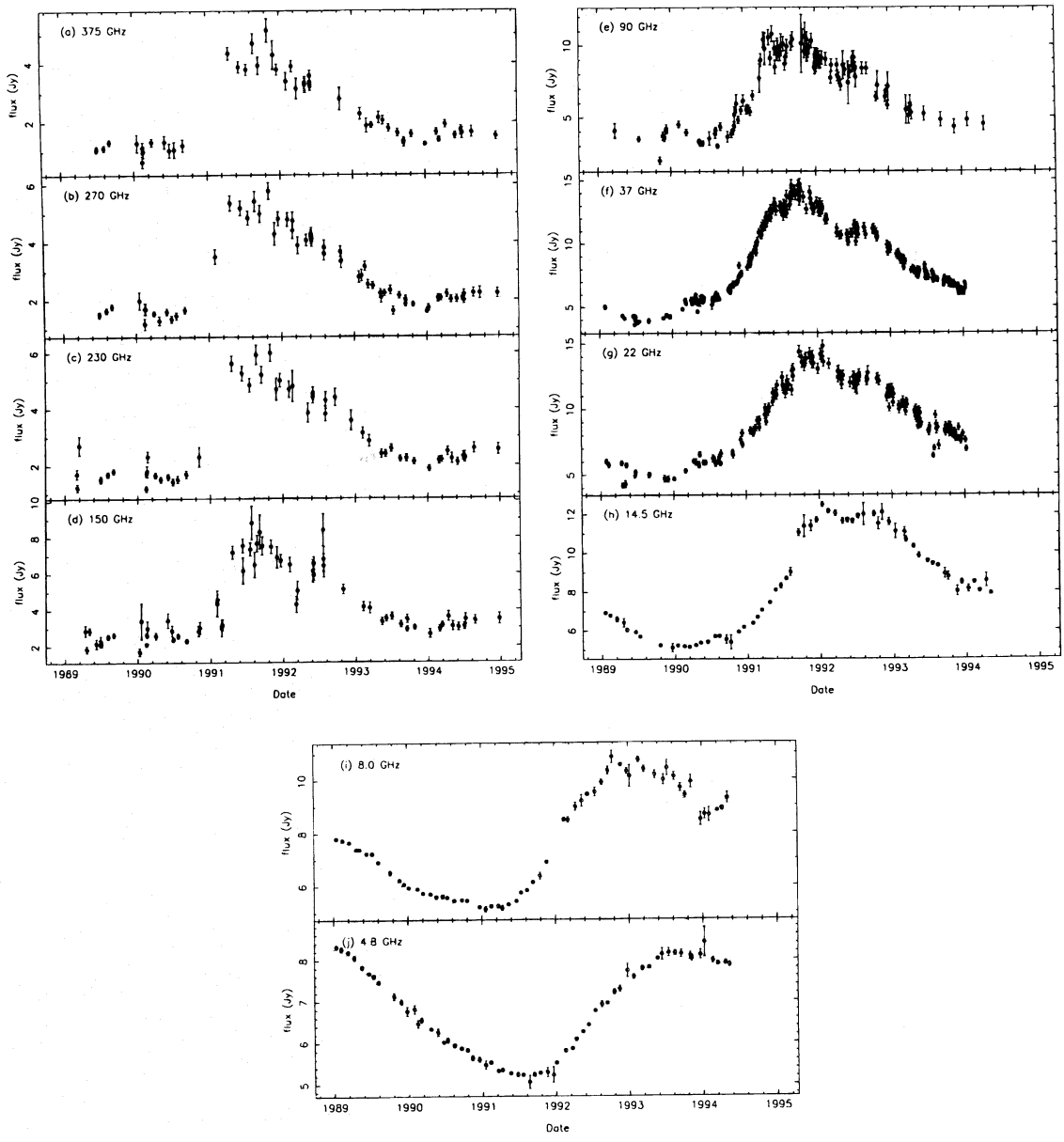

FIG. 1.—Light curves of 1641+399 (3C 345)

© American Astronomical Society • Provided by the NASA Astrophysics Data System

1996ApJ...466..158S

probable that it is a composite of several individual flares. Optical (Schramm et al. 1993) and near-infrared (Litchfield, Robson, & Stevens 1994) light curves show the multiple nature of the outburst more clearly.

Between 375 and 37 GHz the data streams peak at approximately the same time (i.e., late 1991), but time delays exist between the 375–37 GHz emission and that at lower frequencies. Application of a formal discrete correlation function or DCF (Edelson & Krolik 1988), using the normalization suggested by White & Peterson (1994; see also Litchfield, Robson, & Hughes 1995), yields time delays of 100 (37–22 GHz), 180 (37–14.5 GHz), 440 (37–8.0 GHz), and 650 days (37–4.8 GHz), with typical uncertainties of ~ 50 days. As expected from simple model considerations, the maximum flare amplitude occurs at 37 GHz; the frequency below which time delays become apparent (e.g., Valtaoja et al. 1992).

3.1.1. *Integrated Polarization Data*

It is interesting to investigate the relationship between the flux density monitoring data and the long-term integrated polarization of 3C 345. At present, such a comparison can only be made at 14.5, 8.0, and 4.8 GHz, with the data collected at the University of Michigan (see Fig. 2). Perhaps the most striking feature of these data is that an increase in the flux density produces a decrease in the percentage polarization. In other words, the effect of an outburst, or shock, is to *depolarize* the emission. Furthermore, detailed inspection reveals that local maxima in the percentage polarization often correspond to local minima in the flux density data and vice versa. This effect, most apparent at 14.5 GHz at which the emission is less opaque, emphasizes the complicated variability behavior that underlies the overall rise and decay of the outburst.

The long-term polarization data (Aller et al. 1985) show that the position angle of the polarized emission has a preferred angle of about 30° during relatively quiescent periods. Taken together with the fact that the position angle of the milliarcsecond jet is $-71°$ (Cawthorne et al. 1993a, b), this result implies that the magnetic field of the underlying jet is ordered predominantly parallel to the flow, as determined by VLBI polarization images (e.g., Brown et al. 1994). During flares the position angle has a complicated dependence on flux density (see Fig. 2).

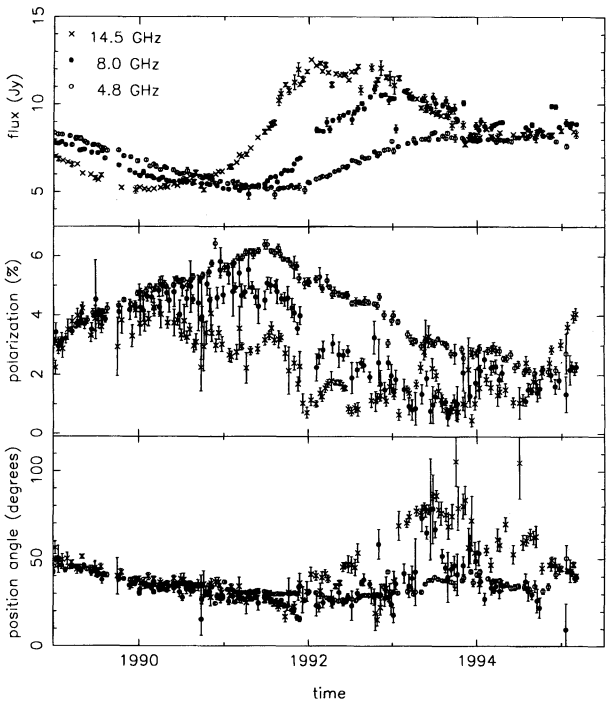

FIG. 2.—Total flux density, integrated percentage polarization, and polarization position angle at 14.5, 8.0, and 4.8 GHz, respectively.

The polarization information thus suggests that shock waves compress a tangled component of the underlying magnetic field in a direction orthogonal to the jet axis. Since a longitudinal component typically dominates during quiescent periods, the net effect is to depolarize the total flux. This conclusion agrees well with the VLBI polarization observations, which show that the maximum fractional polarization occurs *between* the knots (Brown et al. 1994).

3.2. *The Spectra*

Quasi-simultaneous spectra were constructed by linearly interpolating the lower frequency light curves for those dates on which at least two simultaneous JCMT points were available. The resulting spectra for the period 1989 August 8 to 1993 December 31 are presented in Figure 3, and these are discussed briefly here.

The first panel shows evidence for a break in the spectral continuity at around 90 GHz, and this break moves to lower frequency with time, reaching approximately 22 GHz by 1990 November 5 (panel 11). This behavior suggests that the total spectrum is a composite of a high-frequency component that is evolving through the window, along with other decaying and quiescent components. Inspection of the light curves reveals a small "hump" in the emission at around this time (centered on 1990). The peak flux of the high-frequency component initially increases and then remains roughly constant over this period.

The next panel is from 1991 February 2, and at this time the flux has risen dramatically and the turnover has moved to a higher frequency (~ 37 GHz). This spectrum is from an epoch corresponding to the rise of the JCMT light curves (see the 270 GHz light curve). Unfortunately, these light curves are poorly sampled around this period, and, consequently, important information on the rise phase of this large flare was missed. By 1991 April 20, the 375–37 GHz emission has again increased and the new component is clearly dominating the spectrum. The peak flux continues to rise slowly or remains approximately stable for several months, after which it declines. During this period, the turnover frequency moves from 37 GHz (above) to around 14.5 GHz by 1993 February 7 and around 5 GHz by 1993 December 31 (last panel).

3.2.1. *Quiescent Emission and the Flare Spectra*

In order to isolate the spectrum of the flaring component, it is first necessary to subtract the emission from the underlying jet and other components that are assumed to be only slowly variable or "quiescent" (e.g., Marscher & Gear 1985; Valtaoja et al. 1988; Robson et al. 1993). The quiescent spectrum of 3C 345 is presented in Figure 4.

The 375–150 GHz data were binned over the period 1989 March to 1991 January. As discussed above, there is some structure present in the light curves during this period, but it will be smoothed by the binning process. The 375–150 GHz optically thin quiescent spectral index is -0.76 ± 0.11. At lower frequency there is no prolonged

© American Astronomical Society • Provided by the NASA Astrophysics Data System

1996ApJ...466..158S

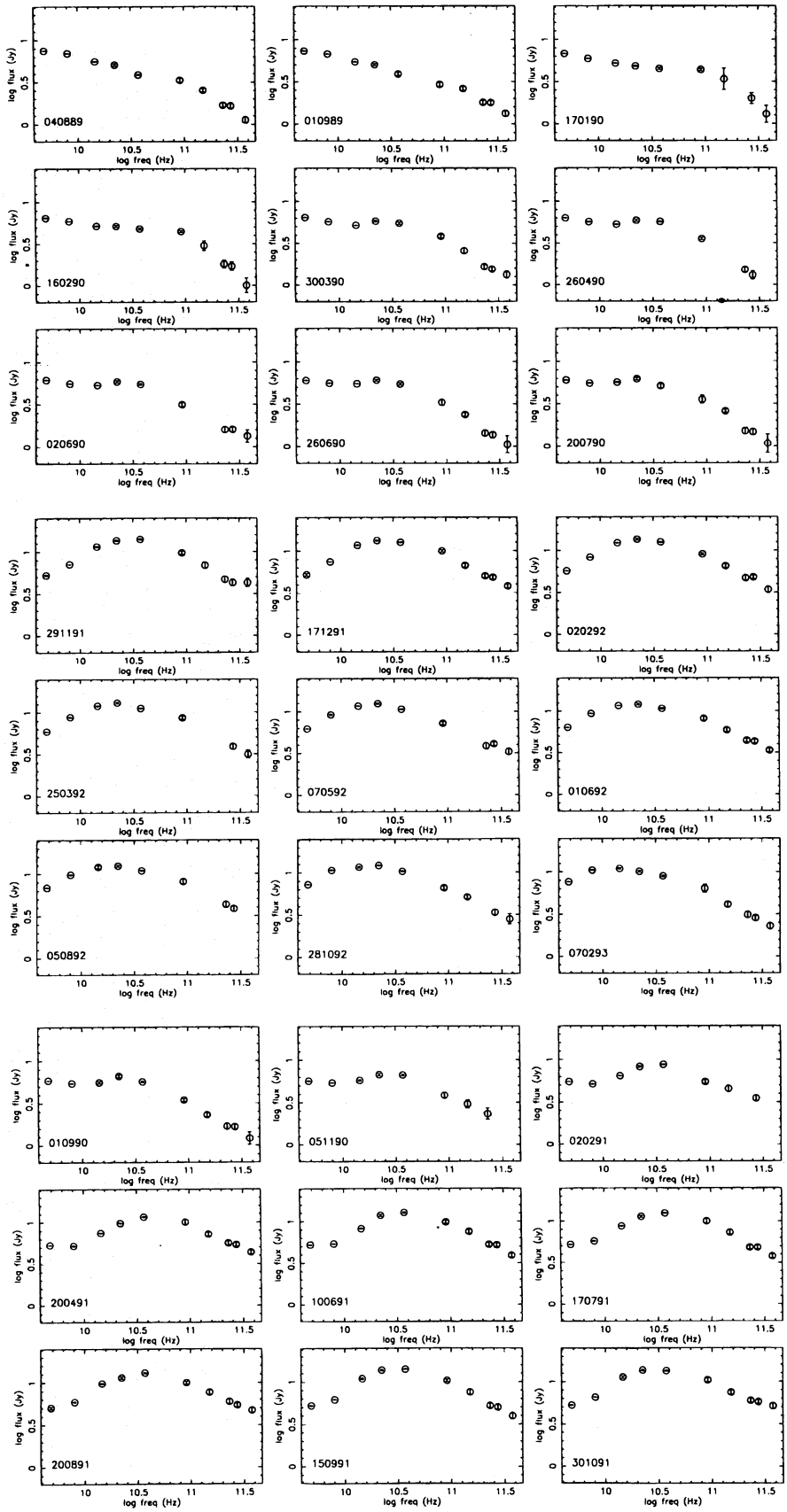

FIG. 3.—Quasi-simultaneous, linearly interpolated spectra of 1641 + 399 (3C 345). Dates indicate the epoch of the JCMT observations.

© American Astronomical Society • Provided by the NASA Astrophysics Data System

1996ApJ...466..158S

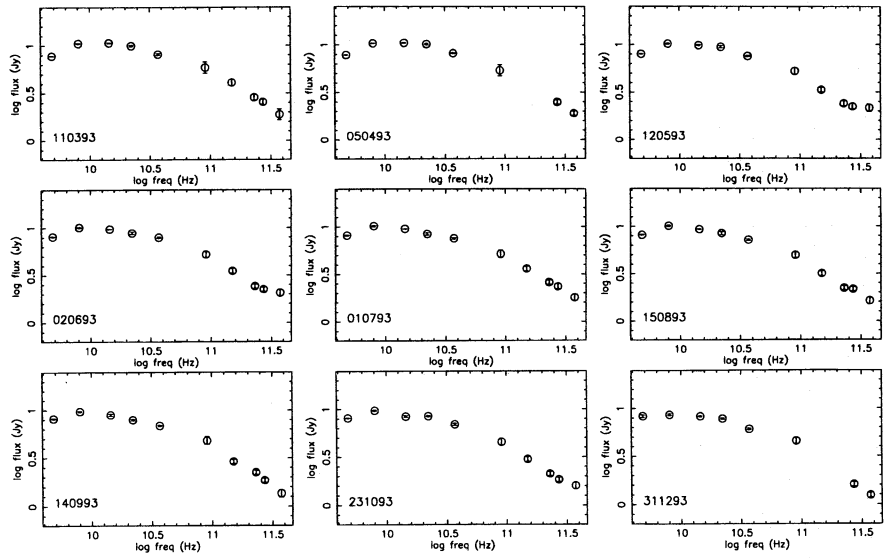

FIG. 3—*Continued*

period of quiescent emission, and so only the lowest point was chosen. Error bars represent the standard deviation of the data in each bin for the 375–150 GHz data, and for the lower frequencies they represent the uncertainties in each individual data point. It is highly probable that increased response times result in the lower frequency emission not reaching the quiescent level before the source flared again. The quiescent spectrum contains discontinuities that suggest that this is the case. Thus, on subtracting the quiescent fluxes from the composite spectrum, the residual emission from the previous decaying component was also removed. This is desirable since it allows the spectrum of the new flaring component to be better isolated. As the flux of the decaying component continues to decline, however, the quiescent level will be systematically overestimated. This effect, although probably small in most cases, may be important at 4.8 GHz during the later stages of the analysis. It should be noted that the last date on which quiescent subtraction was performed was 1993 August 15. Several different quiescent spectra were constructed, and it was found that the results presented below are not affected significantly by small variations in the low-level fluxes.

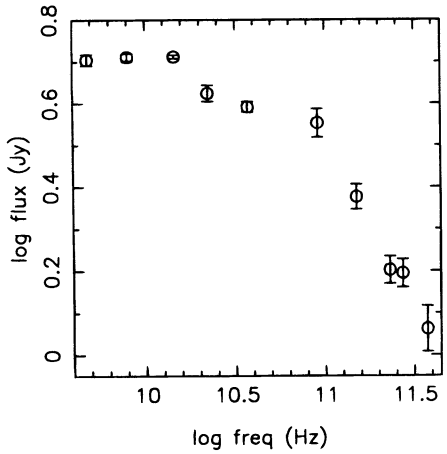

FIG. 4.—Quiescent spectrum of 3C 345

After subtraction of the quiescent spectrum, the resulting flare spectra were fitted with simple homogeneous synchrotron curves. In this manner, the peak flux, peak frequency, and electron spectrum can be determined analytically (e.g., Stevens et al. 1995; see Table 1). The fits are shown in Figure 5. An important result is that the spectrum of the flaring component, which is identified with the shock emission, is well fitted by the adopted synchrotron curve. This means that the emitting region is essentially homogeneous, at least during the first year or so of its evolution (i.e., the optically thick spectral index is +2.5). The results support the process of quiescent subtraction (and the chosen quiescent spectrum) since the outcome is so straight forward and is as expected from basic synchrotron theory.

Previous work has also strongly indicated that the flare spectrum in blazars is that of a simple homogeneous source.

TABLE 1

HOMOGENEOUS SYNCHROTRON CURVE FITS TO THE FLARE SPECTRA

Epoch	Date	log (ν_m) (Hz)	log (S_m) (Jy)	s[a]	α[b]
1.....	200491	10.60	0.886	1.91	−0.45
2.....	100691	10.54	0.958	2.13	−0.56
3.....	170791	10.51	0.937	2.09	−0.55
4.....	200891	10.50	0.957	1.91	−0.45
5.....	150991	10.46	1.025	2.17	−0.58
6.....	301091	10.45	0.999	1.91	−0.46
7.....	291191	10.42	1.010	2.09	−0.55
8.....	171291	10.38	0.962	1.96	−0.48
9.....	020292	10.34	0.926	...	...
10.....	250392	10.30	0.892	...	...
11.....	070592	10.26	0.848	...	...
12.....	010692	10.23	0.830	...	...
13.....	050892	10.21	0.930	...	...
14.....	281092	10.15	0.901	...	...
15.....	070293	10.07	0.815	...	...
16.....	110393	10.04	0.775	...	...
17.....	050493	10.04	0.751	...	...
18.....	120593	10.00	0.730	...	...
19.....	020693	9.98	0.706	...	...
20.....	010793	9.96	0.691	...	...
21.....	150893	9.95	0.690	...	...

[a] Electron energies are distributed as E^{-s}.
[b] The spectral index $\alpha = (1 - s)/2$.

© American Astronomical Society • Provided by the NASA Astrophysics Data System

1996ApJ...466..158S

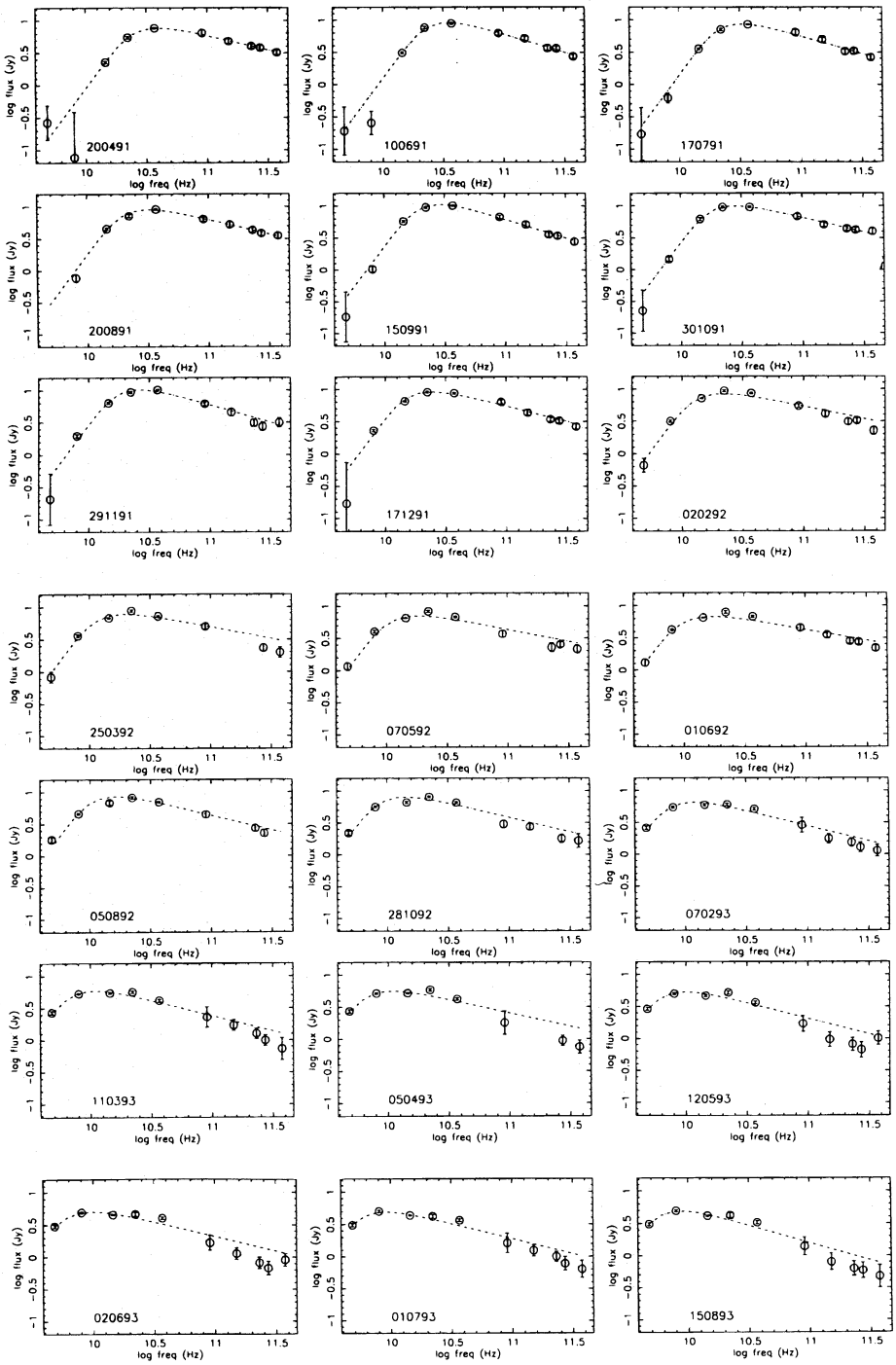

FIG. 5.—Quiescent subtracted spectra, which are fitted with homogeneous synchrotron curves

For a large outburst in the quasar 1921−293, Dent & Balonek (1980) found that the initial optically thick spectral index was ~2 below 15 GHz. The radio spectrum of both 3C 84 (O'Dea, Dent, & Balonek 1984) and NRAO 140 (Marscher 1988) has been deconvolved into several homogeneous components. Valtaoja et al. (1988) found that the composite of all flare spectra in a sample of compact radio sources was well fitted by a homogeneous spectrum.

Van der Walt (1993) has argued that the process of quiescent subtraction is not justified. It was suggested that the flare emission replaces some of the emission from the underlying flow, resulting in subtraction of the incorrect base level. In this scenario, the flaring region expands to occupy a large part of the jet, thus making the quiescent level time dependent. The results presented above show that this effect is not important over the frequency range considered. For 3C 345, the flare spectrum can be fitted with a homogeneous form for more than 2 yr after the initial flare rise, and over much of this period the spectral evolution is consistent with expansion losses being the dominant energy loss mechanism (see Table 1 and § 3.4). Thus, it is likely that the shocks are intrinsically thin, as suggested by Marscher & Gear (1985), and that they remain so for periods of a few years or more.

It is clear from the 3C 345 flare spectra (Fig. 5) that the high-frequency, optically thin emission deviates from the

© American Astronomical Society • Provided by the NASA Astrophysics Data System

1996ApJ...466..158S

homogeneous form with time. The points fall progressively further and further below the curve. These data have less weight in the fits since the errors are typically much larger than those at lower frequencies. Thus, it is unlikely that the fitted position of the turn over was affected significantly. Table 1 only includes values of s and α for the first eight epochs, since these show little deviation from the curve. The most likely explanation for this effect is that the relativistic electrons in the shock are suffering radiative losses, which result in spectral steepening. This point is discussed further in the next section.

3.3. *Energy Losses*

The emitting electrons in the jet are expected to lose energy. The nature of these losses determines the movement of the flare spectrum with time (Marscher & Gear 1985; see below). In addition, energy losses due to the inverse-Compton and synchrotron processes modify the electron energy distribution and result in a "break" or "cut off" in the high-frequency optically thin spectrum, which moves to lower frequency with time. Both processes produce identical changes to the spectral shape.

If the electrons are constantly injected into or reaccelerated in a magnetic field with spectrum KE^{-s}, then at low (but still optically thin) frequencies, where energy losses are unimportant, the spectral slope is given by $(1 - s)/2$. From Table 1 it can be seen that the initial value of s deduced from the fits is about 2, leading to a spectral index of about -0.5. Above the break frequency, radiative losses steepen the spectrum to $-s/2 \sim -1$ (Kardashev 1962). Alternatively, in the case of an instantaneous burst of injection or reacceleration of electrons that subsequently lose energy radiatively, the spectrum steepens from $(1 - s)/2$ to $-(2s + 1)/3 \sim -1.66$ (Kardashev 1962). This result is strictly true only if the pitch angle distribution is isotropic. In a jet, electrons with small pitch angles may be scattered to large pitch angles by plasma instability or magnetic field turbulence. In this case, the spectrum can steepen further since electrons with large pitch angles will lose their energy faster.

To investigate further the possibility that radiative losses are steepening the optically thin shock spectra, a plot of the 270–90 GHz two-point spectral index was made against 270 GHz flux (Fig. 6). These spectral indices were constructed by taking each 270 GHz flux measurement over the period of interest and linearly interpolating the 90 GHz light curve. Quiescent fluxes were subtracted to obtain the flare spectral index. Note that the emission at 90 and 270 GHz is always optically thin over the period considered, i.e., the decay of the large outburst from 1991 April to 1994 April.

It is clear that there exists a strong correlation of increasing spectral steepness with decreasing flux; the spectral index is also steepening with time, since it is the flare decay that is being investigated. There is evidence for the break frequency to move to lower frequency with time, as expected (Fig. 5), although the effect is difficult to quantify. The spectral index becomes steeper than the value of -1, which is expected from continuous injection or reacceleration of electrons. The data are more consistent with an instantaneous injection or reacceleration of electrons that subsequently suffer radiative losses. If this is the case, then the shock wave is formed by injection into the jet of a burst of electrons that decay radiatively while undergoing little reacceleration. This conclusion was reached independently from analysis of VLBI polarization data (Wardle et al. 1994).

3.4. *Evolution of the Flare Spectrum*

The Marscher & Gear model predicts the evolution of the flare spectrum on the (S_m, ν_m) plane. The model comprises three phases that correspond to the three energy loss mechanisms (inverse-Compton, synchrotron, and expansion losses) that are in operation, one being dominant at any given time. The turnover frequency, ν_m, is predicted to move toward lower frequency with time, as the emitting region expands along the jet. During the Compton (rise) phase S_m increases, in the synchrotron (plateau) phase S_m remains approximately constant, and during the adiabatic (decay) phase S_m decreases (see Marscher & Gear 1985 for the exact relations for the power-law indices during these phases). A more mathematical approach is also considered in § 4.

The spectral data from Table 1 are now analyzed in more detail. Figure 7 shows the peak flux versus peak frequency. The first point to note is that a power law is clearly a good fit to the (S_m, ν_m) relationship. The slopes of the dashed lines are (from right to left) -0.86 (rise), 0.96 (decay), and 0.98 (decay); it is not clear whether the second rise is a continuation of the previous decay. The second rise occurred

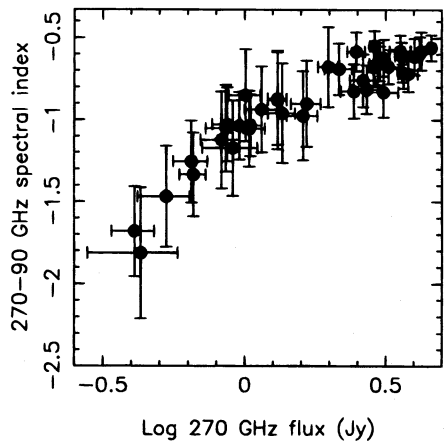

FIG. 6.—270–90 GHz two-point spectral index vs. logarithm 270 GHz flux. Quiescent level fluxes have been subtracted.

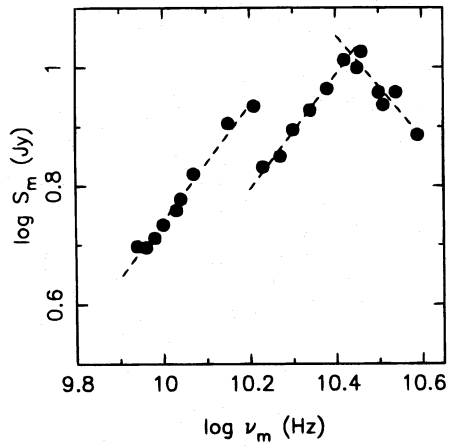

FIG. 7.—Logarithmic evolution of the peak flux with peak frequency. Data are from Table 1. The gradients of the dashed lines are (from right to left) -0.86 (rise), 0.96 (decay), and 0.98 (decay).

© American Astronomical Society • Provided by the NASA Astrophysics Data System

1996ApJ...466..158S

between 1992 June and 1992 August and is probably associated with the small rise in the light curves from this period (Fig. 1). If this rise is assumed to be another flare, then both flares have the same gradient during the decay phase, i.e., ~ 1. The nature of these decays is investigated in the next section.

The initial rise is probably not connected with the proposed Compton phase of the flare evolution. As discussed previously, the light curves were poorly sampled at the highest frequencies during the rise of the large outburst, leading to a gap of about 8 months in the observations. It is likely that the Compton phase is much more rapid than this. The lack of spectral steepening during this rise (see Table 1) also suggests that it was not driven by radiative energy losses. In this case, the dominant energy loss mechanism must be adiabatic expansion, but for a straight jet, the flux is predicted to decrease with decreasing frequency. This leads to the conclusion that the jet must bend toward the line of sight during this period (see also § 4.2), i.e., the increase in turnover flux is produced by Doppler enhancement (see, e.g., Marscher, Gear, & Travis 1992). Support for this finding comes from VLBI observations, which show that the jet is curved on all scales, particularly close to the core where the millimeter emission is thought to arise (e.g., Bååth et al. 1992; Krichbaum et al. 1993; Zensus, Cohen, & Unwin 1995).

Also of interest is the evolution of S_m and ν_m with time (Figs. 8 and 9, respectively). The time, $t = 0$, was chosen to be 1990 September 1, which is the epoch of observation immediately preceding the rise of the JCMT light curves. Figure 8 has a similar form to Figure 7, again suggesting that two flares occurred during the period of interest. The dashed line is a fit to the second decay and has a slope of -1.5. The continuous curve of Figure 9, however, demonstrates that ν_m evolved smoothly toward lower frequency. This spectral behavior is similar to that observed in 0420−014 (Stevens et al. 1995). A rejuvenation of the former event is a possible explanation; although, since the peak flux rises once more, a bend in the jet directing the emission closer to the line of sight is again a likely possibility.

It is clear that a power law is not a good approximation to the evolution of ν_m with time over the entire period. Indeed, Figure 9 indicates that the rate at which ν_m evolves to lower frequency slows down. This effect is more apparent

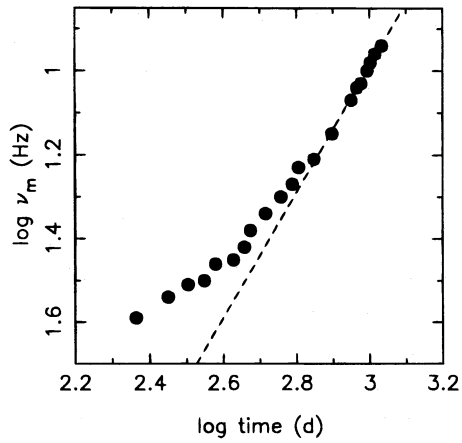

FIG. 9.—Logarithmic evolution of the peak frequency with time. The dashed line has gradient ~ -1.5.

if ν_m is plotted against time rather than the logarithm of time, as shown in Figure 10 (see § 4 for further comment on this point). The trend of Figure 9 can locally be approximated by a power law, and a fit to the last nine points (coincident with the second decay) yields a slope of -1.5. The two slopes of -1.5 for log S_m and log ν_m versus log time are thus consistent with the observed relationship, $S_m \propto \nu_m^{1.0}$, for the second decay.

4. COMPARISON WITH THE MARSCHER & GEAR MODEL

The Marscher & Gear model considers the passage of a shock wave along a conical, adiabatic relativistic jet that is aligned toward the observer. Relativistic electrons with a power-law distribution of energies given by $N(E)dE = KE^{-s}dE$ are injected at a point R_0, after which the plasma flows outward with a constant bulk Lorentz factor, Γ. Shock waves are expected to form if the pressure or bulk velocity of the flow increase significantly. The magnetic field, B, and parameter, K, are assumed to fall off radially, with $B \propto R^{-a}$ and $K \propto R^{-b}$. The parameter a is equal to 1 for a magnetic field oriented perpendicular to the flow, while $a = 2$ for a field aligned along the flow. For an adiabatically expanding jet, $b = 2(s + 2)/3$ (Marscher 1980).

As described in the previous section, the model predicts the evolution of the synchrotron spectrum for three cases

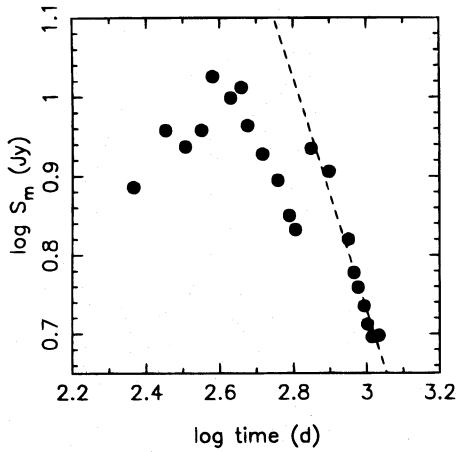

FIG. 8.—Logarithmic evolution of the peak flux with time. The gradient of the dashed line is ~ -1.5.

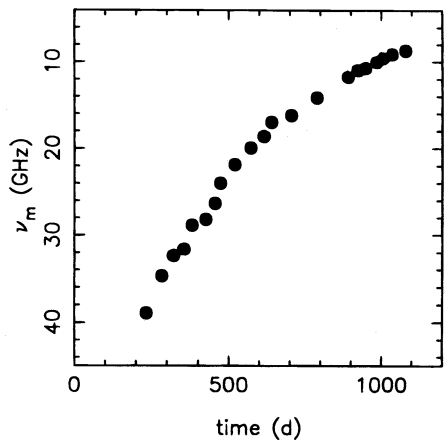

FIG. 10.—Evolution of the peak frequency with time. Note how the gradient of the curve changes with time.

© American Astronomical Society • Provided by the NASA Astrophysics Data System

1996ApJ...466..158S

that correspond to the dominant electron energy-loss mechanism. Lack of spectral steepening during the early rise phase of the flare led to the conclusion that the jet must bend toward the line of sight at this time. The subsequent steepening discussed in § 3.3 must have little effect on the evolution of the flare spectrum, since the movement is consistent with the adiabatic expansion phase and not the synchrotron or Compton phases. In this case, we can postulate that the observed spectral steepening was produced at an earlier epoch, when the emitting region was more compact, and that subsequent expansion shifted the break into the millimeter part of the spectrum. If this scenario is correct, then it is consistent with the idea that the inverse Compton X-ray and γ-ray emission is produced from the optical/UV synchrotron electrons (e.g., Maraschi et al. 1994).

For $a = 1$ and $s = 2$, the shock model predicts that for the adiabatic phase $S_m \propto \nu_m^{0.45}$ (see Marscher & Gear 1985). The observations show that the actual decay is more rapid than the model predicts. VLBI observations of 3C 345 at 5 GHz show that the milliarcsecond jet curves gently away from the line of sight (e.g., Wardle et al. 1994), and therefore we may expect the flux to be diminished by the Doppler effect during the later stages of the flare, consistent with the rapid decay. However, Valtaoja et al. (1988) found that the decay of a number of flares in a sample of 10 or so blazars followed $S_m \propto \nu_m^1$, exactly as found here for 3C 345, and so a more general explanation may have to be sought. In fact, many blazar jets appear to curve (e.g., Krichbaum et al. 1993, 1994), and if we assume that in these cases the jet is initially oriented quite close to the line of sight, then it may be expected that any curvature is most likely to be away from us.

In this section, adaptations of the Marscher & Gear model are used to explain the rapid decay of the flares. Two cases are considered: (1) a straight jet for which the flow is not assumed to be adiabatic and in which the magnetic field orientation is not fixed, and (2) a curved adiabatic jet, again with no assumed magnetic field orientation.

Following Marscher & Gear (1985), the shock thickness, x, is assumed to be proportional to R during the adiabatic phase. For 3C 345, $s = 2$ was found, and this value is adopted throughout. The magnetic field orientation is not fixed, therefore a is left as a free parameter. Standard synchrotron formulae (e.g., Pacholczyk 1970) give for the flux density, S_ν, and peak frequency, ν_m,

$$S_\nu \propto KB^{(s+1)/2}R^2x\delta^{(s+3)/2}\nu^{(1-s)/2}, \quad (1)$$

$$\nu_m \propto [KB^{(s+2)/2}x\delta^{(s+2)/2}]^{2/(s+4)}. \quad (2)$$

These equations can be rewritten in terms of R and ν by substituting the dependences of B, K, and x on R. The Doppler factor will be constant for a straight jet, but it will be a function of R if the jet curves with respect to the line of sight (see § 4.2).

4.1. *Case 1: A Straight Nonadiabatic Jet*

In this case, b is a free parameter, and so, by substituting the dependences of B, K, and x on R into equations (1) and (2), the following relations can be obtained:

$$S_\nu \propto R^{3-b-a(s+1)/2}\nu^{(1-s)/2}, \quad (3)$$

and

$$\nu_m \propto R^{-[2b+a(s+2)-2]/(s+4)}. \quad (4)$$

Combining equations (3) and (4) gives

$$S_m \propto \nu_m^{[5b+3a-13+2s(a-1)]/[2b+a(s+2)-2]}, \quad (5)$$

where $S_m \equiv S_\nu(\nu_m)$. The dependence of S_m on time can be found by combining equations (3) and (4) and noting that R is expected to be proportional to time, t (Rees 1967):

$$S_m \propto t^{[13-3a-5b-2s(a-1)]/(s+4)}. \quad (6)$$

The dependence of ν_m on time is simply equation (4) with t substituted for R:

$$\nu_m \propto t^{-[2b+a(s+2)-2]/(s+4)}. \quad (7)$$

The theoretical predictions can now be compared to the observational dependences derived in the previous section. Equating the exponents of equations (5), (6), and (7) with 1.0, -1.5, and -1.5, respectively, and substituting $s = 2$ gives

$$a + b = 5, \quad (8)$$

$$5b + 7a = 26, \quad (9)$$

$$b + 2a = 5.5. \quad (10)$$

These equations, rather fortuitously given the uncertainties in the analysis, yield an analytical solution at $a = 0.5$ and $b = 4.5$. It is difficult to estimate formal errors on the values of a and b, but applying small uncertainties to the values of the slopes derived from Figures 7, 8, and 9, the values $0 \le a \le 1$ and $4 \le b \le 5$ appear reasonable.

The first point to note is that the value of b obtained from the analysis is much larger than that expected for an adiabatic flow, where $b = 2(s + 2)/3 = 8/3$ for $s = 2$. In this case, the assumption that the jet is adiabatic is possibly not justified. The most probable explanation is that the radiative (synchrotron and inverse-Compton) losses suffered by the electrons have a significant effect on the jet energetics. Second, the allowed range of a indicates that the magnetic field is ordered perpendicular to the jet direction, since, in this case, $a = 1$. This is the magnetic field orientation that is expected to arise if shock waves compress the underlying field. Allowed values of $a < 1$ suggest that the field is also undergoing regeneration due to turbulent processes (Hughes et al. 1989a).

4.2. *Case 2: A Curved Adiabatic Jet*

In this section, we investigate whether a curved jet can account for the observed rapid decay of the flares. It is assumed that the Doppler factor varies with distance down the jet as a power law, with $\delta \propto R^{-c}$, and that the flow is adiabatic. Thus, in a similar manner to that described in the previous section, equations (1) and (2) reduce to

$$S_\nu \propto R^{[2(5-2s)-3a(s+1)-3c(s+3)]/6}\nu^{(1-s)/2}, \quad (11)$$

$$\nu_m \propto R^{-[2(2s+1)+3(a+c)(s+2)]/[3(s+4)]}, \quad (12)$$

$$S_m \propto \nu_m^{[(4s-19)+3a(2s+3)+3c(3s+7)]/[2(2s+1)+3(a+c)(s+2)]}. \quad (13)$$

These equations have been derived previously (Marscher 1990). The dependences of S_m and ν_m on time are

$$S_m \propto t^{-[3c(3s+7)+3a(2s+3)+(4s-19)]/[3(s+4)]}, \quad (14)$$

$$\nu_m \propto t^{-[2(2s+1)+3(a+c)(s+2)]/[3(s+4)]}. \quad (15)$$

Substituting $s = 2$ and equating the power-law indices of equations (13), (14), and (15) with the corresponding obser-

© American Astronomical Society • Provided by the NASA Astrophysics Data System

1996ApJ...466..158S

vational values gives

$$9a + 27c = 21 , \quad (16)$$

$$12a + 12c = 17 , \quad (17)$$

$$21a + 39c = 38 . \quad (18)$$

These equations have an analytical solution at $a = 23/24 = 0.96$, $c = 11/24 = 0.46$, with similar errors to those proposed in the previous section.

As found for case 1, the results of this analysis favor a magnetic field orientation that is perpendicular to the jet direction. The required value of c shows that the jet must curve *away* from the line of sight. Since the dependence of Doppler factor on distance down the jet is weak, this curvature is gentle, as found previously (Wardle et al. 1994). If the jet makes an angle of 2° to the line of sight (θ; Wardle et al. 1994) at 5 pc, then assuming a constant bulk Lorentz factor of $\Gamma = 10$ gives $\theta \sim 6.^{\circ}1$ at 20 pc. In § 3.4, it was suggested that the initial rise was caused by the jet bending toward the line of sight during this period. If the jet is adiabatic, then equation (13) shows that an index $c \sim -2.8$ is required to produce the observed trend of S_m with ν_m, implying that the jet curved rather strongly toward us at this earlier stage.

In § 3.4, it was also found that the rate at which ν_m evolves toward lower frequency slows down with time. This behavior is predicted by both case 1 and case 2. In fact, by differentiating equation (7) or (15) with respect to time, it can be shown that, for reasonable positive values of a, b, and c (such as those found above), $d\nu_m/dt \rightarrow 0$ as $t \rightarrow \infty$.

5. SUMMARY

The importance of centimeter–submillimeter observations to the testing and development of models for the emission from blazars has been demonstrated. It is in this frequency range that the flare (or shock) spectrum typically becomes self-absorbed; the higher frequency data are crucial in that they allow estimation of the optically thin (and thus electron) spectrum.

The relatively smooth nature of the variability of 3C 345 over the period of investigation greatly aided the analysis. Clearly it is imperative that the quiescent level can be identified, but it is also important that the source does not undergo repeated flaring on timescales of, say, less than 1 yr. In this case, difficulties in isolating a single flare spectrum ensue, as was the case for 3C 273 (Robson et al. 1993) and 3C 279 (Litchfield et al. 1995). One problem, however, is that the rise of the flares is often rather abrupt (weeks in some cases) and as such was often missed at the highest frequencies due to the nature of the sampling. The study of the early phases of the flare evolution was hampered in this manner, which is unfortunate since it is the growth phase of the flares that is least understood. A revised observing strategy is required to allow adequate sampling of the rise phase of flares. The major conclusions of this work are summarized below:

1. It has been suggested that the flaring and quiescent components cannot be separated in a simple way, since, during an outburst, the quiescent emission is time dependent (van der Walt 1993). This work, however, strongly indicates that quiescent subtraction is a valid process over the frequency range considered because the resulting flare spectrum is that of a homogeneous synchrotron source. If the shocks are physically thin, as suggested by Marscher & Gear (1985), then the spectrum may well be expected to have this form. The advantage of finding such a simple flare spectrum is that the peak flux and peak frequency can be determined analytically, whereas in the past, resort was made to more primitive methods of identifying the turn over. The flare spectrum could be fitted adequately by a homogeneous source for a period of about 2 yr. This result implies that the flaring region does not become significantly inhomogeneous due to expansion, which would result in a broadening of the turnover. The evolution of the turnover as the flare develops can, thus, easily be investigated.

2. The initial optically thin flare spectral index was found to be roughly -0.5, which is similar to previous estimates (Valtaoja et al. 1988, and references therein). It is interesting to note that the knots in the jet of the well-studied radio source M87 also have an optically thin spectral index of roughly -0.5 (Biretta, Stern, & Harris 1991; see also Biretta & Meisenheimer 1993). The optically thin flare spectrum steepened with time (as the flux decayed) to the value expected in the case of an instantaneous burst or reacceleration of electrons that subsequently suffered radiative losses. This result suggests that little reacceleration is occurring at the shock front.

3. The evolution of the turnover was compared with the model predictions. The turnover moved smoothly to lower frequency with time, as expected if the emitting region is expanding. This movement was also observed to slow down with time, as predicted. Both the spectral evolution and the light curves suggest that 3C 345 displayed two flares during the period of interest, the second being lower in amplitude and peaking at lower frequency than the first. In fact, the continuity of the spectral evolution from one flare to the other suggests that the second event may have resulted from a rejuvenation of the first. Alternatively, this evolutionary behavior could be due to either a sharp bend in the jet or a change in the shock orientation with respect to the line of sight. Such events could be confirmed with multiepoch, high-frequency VLBI observations and would manifest as a brightening of one of the components, probably the one nearest to the core. Such "flares" in the emission from individual VLBI components have already been observed for two BL Lac objects at 5 GHz (Gabuzda et al. 1994).

4. The data show that a power-law description of the evolution of peak flux with peak frequency is a good one. The initial rise of S_m with ν_m is modeled successfully by an emitting region that expands adiabatically down a jet that bends toward the line of sight. Lack of spectral steepening suggests that the inverse-Compton or synchrotron phases were not responsible for the rise. The decay of the flares was found to be more rapid than predicted, with $S_m \propto \nu_m^{1.0}$. A similar conclusion was reached by Valtaoja et al. (1988) for a number of blazars. In order to reconcile this rapid decay with the model, either the jet has to be nonadiabatic or it has to curve away from the line of sight during the later stages of the outburst. The bending models are consistent with VLBI observations, which show convincing evidence for complex jet curvature.

5. While both of these models describe well the observed trend, it is not immediately clear that the curved jet case could be applied to blazars in general; cf. the Valtaoja et al. (1988) finding that rapid flare decay is not unusual. Many blazar jets do, however, appear to be curved, and if we assume that in these cases the jet is initially oriented quite close to the line of sight, as for 3C 345, then it may be

© American Astronomical Society • Provided by the NASA Astrophysics Data System

1996ApJ...466..158S

expected that any curvature is most likely to be away from us.

6. Both models indicate that the magnetic field of the shock is ordered perpendicular to the flow, as expected from compression of the underlying field. Total polarization monitoring data support this finding; i.e., the polarization is roughly perpendicular ($B_{\|}$) to jet axis during quiescent periods and the effect of the outbursts (shocks) is to depolarize the total emission.

We thank the referee, Alan Marscher, for perceptive comments on the original version of this paper. S. J. L. acknowledges the receipt of a PPARC PDRA. This work made extensive use of the University of Central Lancashire STARLINK node and the JCMT data archive facility. The James Clerk Maxwell Telescope is operated by The Observatories on behalf of the Particle Physics and Astronomy Research Council of the United Kingdom, the Netherlands Organization for Scientific Research, and the National Research Council of Canada. We thank all those involved for the JCMT SERVICE observations that are included in this work. M. F. A. and H. D. A. acknowledge support from the NSF grant AST 94-21979. The BIMA array is operated by the Berkeley-Illinois-Maryland Association, with support from the National Science Foundation grant NSF FD04-13933.

REFERENCES

Aller, H. D., Aller, M. F., Latimer, G. E., & Hodge, P. E. 1985, ApJS, 59, 513
Angel, R., & Stockman, H. 1980, ARA&A, 18, 321
Bååth, L. B., et al. 1992, A&A, 257, 31
Biretta, J. A., & Meisenheimer, K. 1993, in Lecture Notes in Physics, Jets in Extragalactic Radio Sources, ed. H.-J. Röser & K. Meisenheimer (Heidelberg: Springer), 159
Biretta, J. A., Stern, C. P., & Harris, D. E. 1991, AJ, 101, 1632
Brown, L. F., Roberts, D. H., & Wardle, J. F. C. 1994, ApJ, 437, 108
Cawthorne, T. V., & Wardle, J. F. C. 1988, ApJ, 332, 696
Cawthorne, T. V., Wardle, J. F. C., Roberts, D. H., & Gabuzda, D. C. 1993a, ApJ, 416, 519
Cawthorne, T. V., Wardle, J. F. C., Roberts, D. H., Gabuzda, D. C., & Brown, L. F. 1993b, ApJ, 416, 496
Dent, W. A., & Balonek, T. J. 1980, Nature, 283, 747
Duncan, W. D., Robson, E. I., Ade, P. A. R., Griffin, M. J., & Sandell, G. 1990, MNRAS, 243, 126
Edelson, R. A., & Krolik, J. H. 1988, ApJ, 333, 646
Gabuzda, D. C., Mullan, C. M., Cawthorne, T. V., Wardle, J. F. C., & Roberts, D. H. 1994, ApJ, 435, 140
Hughes, P. A., Aller, H. D., & Aller, M. F. 1985, ApJ, 298, 310
———. 1989a, ApJ, 341, 54
———. 1989b, ApJ, 341, 68
Kardashev, N. S. 1962, Soviet Astron., 6, 317
Krichbaum, T. P., et al. 1993, A&A, 275, 375
Krichbaum, T. P., Witzel, A., Standke, K. J., Graham, D. A., Schalinski, C. J., & Zensus, J. A. 1994, in Compact Extragalactic Radio Sources, NRAO Workshop No. 23, ed. J. A. Zensus & K. I. Kellermann (Green Bank: NRAO), 39
Litchfield, S. J., Robson, E. I., & Hughes, D. H. 1995, A&A, 300, 385
Litchfield, S. J., Robson, E. I., & Stevens, J. A. 1994, MNRAS, 270, 341
Litchfield, S. J., Stevens, J. A., Robson, E. I., & Gear, W. K. 1995, MNRAS, 274, 221
Maraschi, L., et al. 1994, ApJ, 435, L91
Marscher, A. P. 1980, ApJ, 235, 386
———. 1988, ApJ, 334, 552
Marscher, A. P. 1990, in Parsec-Scale Radio Jets, NRAO Workshop, ed. A. J. Zensus & T. J. Pearson (Cambridge: Cambridge Univ. Press), 236
Marscher, A. P., & Gear, W. K. 1985, ApJ, 298, 114
Marscher, A. P., Gear, W. K., & Travis, J. P. 1992, in Variability of Blazars, ed. E. Valtaoja & M. Valtonen (Cambridge: Cambridge Univ. Press), 85
Moffet, A. T., Gubbay, J., Robertson, D. S., & Legg, A. J. 1972, in IAU Symp. 44, External Galaxies and Quasi-Stellar Objects, ed. D. S. Evans (Dordrecht: Reidel), 228
O'Dea, C. P., Dent, W. A., & Balonek, T. J. 1984, ApJ, 278, 89
Pacholczyk, A. G. 1970, Radio Astrophysics (San Francisco: Freeman)
Rees, M. J. 1967, MNRAS, 135, 345
Robson, E. I., et al. 1993, MNRAS, 262, 249
Sandell, G. 1994, MNRAS, 271, 75
Schramm, K.-J., Borgeest, U., Kühl, D., Linde, J. V., & Linnert, M. D. 1993, A&A, 278, 391
Steppe, H., et al. 1993, A&AS, 102, 611
Stevens, J. A., Litchfield, S. J., Robson, E. I., Gear, W. K., Teräsranta, H., Tornikoski, M., & Valtaoja, E. 1995, MNRAS, 275, 1146
Stevens, J. A., Litchfield, S. J., Robson, E. I., Hughes, D. H., Gear, W. K., Teräsranta, H., Valtaoja, E., & Tornikoski, M. 1994, ApJ, 437, 91
Stevens, J. A., & Robson, E. I. 1994, MNRAS, 270, L75
Teräsranta, H., et al. 1992, A&AS, 94, 121
Ulich, B. L. 1981, AJ, 86, 1619
Unwin, S. C., Wehrle, A. E., Urry, C. M., Gilmore, D. M., Barton, E. J., Kjerulf, B. C., Zensus, J. A., & Rabaça, C. R. 1994, ApJ, 432, 103
Valtaoja, E., et al. 1988, A&A, 203, 1
Valtaoja, E., Teräsranta, H., Urpo, S., Nesterov, N. S., Lainela, M., & Valtonen, M. 1992, A&A, 254, 71
van der Walt, D. J. 1993, ApJ, 409, 126
Wardle, J. F. C., Cawthorne, T. V., Roberts, D. H., & Brown, L. F. 1994, ApJ, 437, 122
Webb, J. R., et al. 1994, ApJ, 422, 570
Webb, J. R., Smith, A. G., Leacock, R. J., Fitzgibbons, G. L., Gombola, P. P., & Shepherd, D. W. 1988, AJ, 95, 374
White, R. J., & Peterson, B. M. 1994, PASP, 106, 879
Zensus, J. A., Cohen, M. H., & Unwin, S. C. 1995, ApJ, 443, 35

© American Astronomical Society • Provided by the NASA Astrophysics Data System